



# Particles II

Access the latest eBook →

# 11

Advanced  
Optical Metrology

Particles II



**EVIDENT**  
**OLYMPUS**

**WILEY**

## Impact on Biological Systems and the Environment

This eBook is dedicated to the research of Professor David Wertheim.

In collaboration with various groups, Professor Wertheim uses confocal microscopy to analyse the impact of different types of particles on human health and the environment, with a focus on human health-hazardous particles detected with solid-state nuclear track detectors (SSNTD). Download for free, today.

**EVIDENT**  
**OLYMPUS**

**WILEY**

# Spatially Heterogeneous Tubular Scaffolds for In Situ Heart Valve Tissue Engineering Using Melt Electrowriting


Navid Toosi Saidy, Alicia Fernández-Colino, Behzad Shiroud Heidari, Ross Kent, Michael Vernon, Onur Bas, Shane Mulderrig, Andreas Lubig, José Carlos Rodríguez-Cabello, Barry Doyle, Dietmar W. Huttmacher, Elena M. De-Juan-Pardo,\* and Petra Mela\*

Heart valve tissue engineering (HVTE) aims to provide living autologous heart valve implants endowed with regenerative capabilities and life-long durability. However, fabrication of biomimetic scaffolds capable of providing the required functionality in terms of mechanical performance and tunable porosity to enable cellular infiltration remains a major challenge. Here, the additive manufacturing of bioinspired, spatially heterogeneous, tubular scaffolds enclosing the leaflets, inter-leaflet triangles, and their interface for in situ HVTE using melt electrowriting (MEW) is demonstrated. The innovative platform enables the digital fabrication of scaffolds with ad hoc architecture (e.g., tunable location, specific fiber pattern, and orientation) and customizable geometry via a custom-made control software. The user-friendly interface allows for the definition of areas of the scaffold with specific patterns to obtain properties such as tunable J-shaped stress–strain curve and anisotropy typical of the heart valve leaflet, compliant inter-leaflet triangles, and reinforced curvilinear boundary between them. Heterogeneous, tubular, heart valve MEW scaffolds are then embedded with a microporous elastin-like recombinamer (ELR) hydrogel to develop a soft-network composite favoring cell infiltration and ensuring hemocompatibility. The acute systolic hemodynamic functionality of the MEW/ELR composite satisfies the ISO 5840 requirements, under aortic and pulmonary conditions.

## 1. Introduction

Valvular heart disease is the third leading contributor to cardiovascular disorders worldwide, projected to claim up to 23.6 million lives by 2030 and cost the global healthcare systems over \$749 billion by 2035.<sup>[1]</sup> Heart valve tissue engineering (HVTE) aims to overcome the limitations of current mechanical and biological valve prostheses by providing a valve with the ability to grow and remodel with the patient, offering a permanent, regenerative approach.<sup>[2]</sup> A recent shift in focus has been proposed to facilitate the translation of HVTE to the clinic, specifically the shift to in situ tissue engineering via acellular implants, which are designed to be infiltrated by cells in the body in an endogenous regeneration process.<sup>[3]</sup> Research effort has thus been driven toward the challenge of successfully fabricating mechanically suitable scaffolds with adequate porosity to enable cell infiltration. To this end, bioinspired fabrication strategies have attempted

N. T. Saidy, R. Kent, O. Bas, D. W. Huttmacher  
Centre in Regenerative Medicine  
Institute of Health and Biomedical Innovation (IHBI)  
Queensland University of Technology (QUT)  
60 Musk Avenue, Kelvin Grove, Queensland 4059, Australia  
A. Fernández-Colino, S. Mulderrig, A. Lubig, P. Mela  
Department of Biohybrid & Medical Textiles (BioTex)  
AME-Institute of Applied Medical Engineering  
Helmholtz Institute  
RWTH Aachen University  
Forckenbeckstr. 55, 52074 Aachen, Germany  
E-mail: petra.mela@tum.de

 The ORCID identification number(s) for the author(s) of this article can be found under <https://doi.org/10.1002/adfm.202110716>.

© 2022 The Authors. Advanced Functional Materials published by Wiley-VCH GmbH. This is an open access article under the terms of the Creative Commons Attribution-NonCommercial-NoDerivs License, which permits use and distribution in any medium, provided the original work is properly cited, the use is non-commercial and no modifications or adaptations are made.

DOI: 10.1002/adfm.202110716

B. S. Heidari, M. Vernon, B. Doyle  
Vascular Laboratory  
Harry Perkins Institute of Medical Research  
QEII Medical Centre  
Nedlands and Centre for Medical Research and School of Engineering  
The University of Western Australia  
Perth, WA 6009, Australia  
B. S. Heidari, M. Vernon, E. M. De-Juan-Pardo  
T3mPLATE  
Harry Perkins Institute of Medical Research  
QEII Medical Centre  
Nedlands and Centre for Medical Research  
The University of Western Australia  
Perth, WA 6009, Australia  
E-mail: elena.juanpardo@uwa.edu.au  
B. S. Heidari, M. Vernon, B. Doyle, E. M. De-Juan-Pardo  
School of Engineering  
The University of Western Australia  
Perth, WA 6009, Australia  
O. Bas, D. W. Huttmacher  
ARC ITTC in Additive Biomaterials  
Queensland University of Technology  
Musk Avenue, Kelvin Grove, Brisbane, Queensland 4059, Australia

to incorporate some of the key elements of the well-known heart valve structural–functional relationship by creating fibrillar scaffolds, mainly recapitulating the distribution and directionality of collagen fibers to achieve anisotropic leaflets.<sup>[4]</sup>

Among biofabrication techniques, solution electrospinning has attracted widespread attention due to its capacity to produce ultra-fine fibers mimicking collagen fibrils.<sup>[5]</sup> However, a major drawback of electrospun fibrous scaffolds is the limited capability to support cell infiltration, because of the dense fibrous structure, resulting in insufficient porosity. Recent *in vivo* studies on tissue-engineered valves have confirmed this as a major issue,<sup>[6]</sup> showing unwanted deposition of extracellular matrix (ECM) mainly on the outer surfaces with consequent valve thickening and stenosis and potentially the loss of cell-fiber interactions.<sup>[7]</sup> In addition, the capability of tuning fiber architecture spatially using electrospinning is limited and relies either on the collector geometry and material composition,<sup>[8]</sup> or on the sequential repetition of the spinning process with different rotational axes.<sup>[9]</sup>

Melt electrowriting (MEW) is a high-resolution biofabrication strategy that enables the digital fabrication and additive manufacturing of fibrous scaffolds. MEW provides significant advantages compared to other fiber-forming techniques such as conventional electrospinning, as it permits the accurate deposition of micrometer-scale fibers, enabling tunable mechanical properties, macro-porosities, and patterns for a wide range of uses, including implant tissue engineering,<sup>[10]</sup> and disease modeling.<sup>[11]</sup> Still, using MEW to engineer complex tissues enclosing different regions with specific structural properties, like native heart valves, additionally requires the incorporation of spatial complexity into the design. This remains to be explored to advance the MEW technology to its full potential.

In this work, we present an innovative MEW platform that allows the user to manufacture highly tunable, spatially heterogeneous, fibrous tubular scaffolds with controlled mechanical properties for heart valve tissue engineering. The intuitive user interface enables a quick and easy definition of various architectures throughout multiple regions such as the leaflets, the inter-leaflet triangles, and their interface. We then composited the obtained macro-porous MEW construct with a biologically favorable elastin-like recombinamer (ELR) hydrogel to provide

tailored microporosity, optimized for cellular infiltration. The result is a one-of-a-kind tissue-engineered heart valve benefiting from both classes of scaffolds, with an adequate acute systolic hemodynamic performance under aortic and pulmonary conditions satisfying the ISO standard.

## 2. Results and Discussion

### 2.1. Fabrication and Mechanical Characterization of Tubular Scaffolds

We used an in-house MEW system equipped with a mandrel collector to fabricate various tubular medical-grade poly( $\epsilon$ -caprolactone) (PCL) MEW scaffolds.<sup>[12]</sup> To enable the micro-step movement of the mandrel and therefore the spatial control of fiber placement on the tubular collector, we mounted a stepper motor and a gearing system (Figure 1a). We first designed and printed exemplary monophasic scaffolds including rectangle, diamond, and serpentine fiber architectures (Figure 1bi–iii), which can be combined to make multiphasic and thus heterogeneous, constructs as exemplary shown with a biphasic rectangle and diamond scaffold (Figure 1biv). The accuracy of fiber deposition was confirmed by morphological analysis of Scanning Electron Microscopy (SEM) images (Figure S1, Supporting Information).

Biaxial tensile testing was performed to investigate the mechanical properties of different monophasic designs. Figure 1c illustrates the stress-strain responses of each of the presented scaffold architectures. A J-shaped, stress-strain behavior was exhibited by the serpentine structure, in agreement with our previously reported results obtained with biomimetic flat scaffolds.<sup>[13]</sup> Both the rectangle and diamond patterns exhibited a linear stress–strain response. In addition, each scaffold design demonstrated anisotropic mechanical properties (Figure 1d,e) with respect to the circumferential and longitudinal directions. For the serpentine and rectangle designs, this can be explained by the variation in fiber spacing, where more densely packed fibers create a smaller pore size in the circumferential orientation, resulting in larger linear elastic moduli and ultimate tensile strength in that direction. For the diamond design however, the interior angles are the main contributing factor to the anisotropic mechanical response.

The software platform was programmed to generate continuous patterns, as required by MEW printers, based on the user input while minimizing undesired overlapping of fibers between regions. Combination of the patterns was achieved in a continuous manner so that one region was contiguous with the other within each layer. This method provides a versatile platform allowing the fabrication of heterogeneous tubular scaffolds with the ability to tailor mechanical properties throughout multiple regions of the tube.

### 2.2. Spatially Heterogeneous Scaffolds for Heart Valve Tissue Engineering

Native heart valves are characterized by their non-linearity,<sup>[14]</sup> viscoelasticity,<sup>[15]</sup> and high degree of structural and mechanical heterogeneity.<sup>[16]</sup> Distribution and directionality of major ECM components, primarily collagen fibers, as well as elastin and

J. C. Rodríguez-Cabello  
Bioforge Lab  
University of Valladolid  
CIBER-BBN  
Paseo de Belen 11, Valladolid 47011, Spain

D. W. Huttmacher  
Institute for Advanced Study  
Technical University of Munich  
D-85748 Garching, Germany  
E. M. De-Juan-Pardo  
Mechanical  
Medical and Process Engineering  
Queensland University of Technology  
Musk Avenue, Kelvin Grove, Brisbane, Queensland 4059, Australia  
P. Mela  
Medical Materials and Implants  
Department of Mechanical Engineering and  
Munich Institute of Biomedical Engineering  
Technical University of Munich  
Boltzmannstr. 15, 85748 Garching, Germany

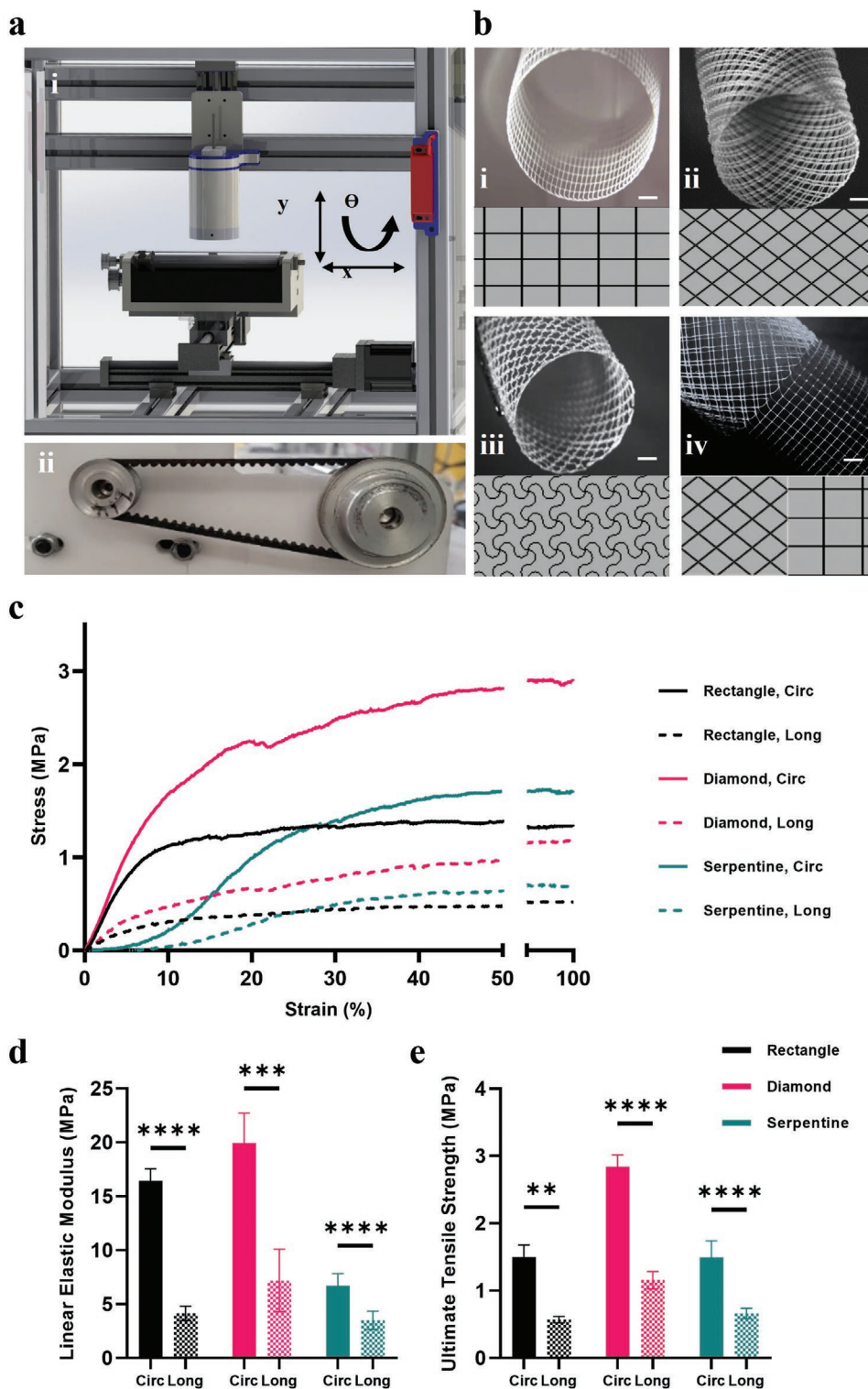


**Figure 1.** ai) 3D model of the MEW device with the modified mandrel collector setup, ii) the in-house mandrel setup with 2:1 gear ratio. b) Exemplary printed monophasic scaffolds with i) rectangle, ii) diamond, and iii) serpentine fiber architectures, as well as iv) exemplary biphasic scaffold, scale bars = 2 mm. c) Exemplary biaxial stress-strain curves for each monophasic scaffold design. d) Linear elastic modulus, and e) ultimate tensile strength of each monophasic scaffold design (average over  $n = 4$  samples for each scaffold design, error bars represent standard deviation,  $**p \leq 0.01$ ,  $***p \leq 0.001$ ,  $****p \leq 0.0001$ ).

glycosaminoglycans, are responsible for the anisotropic and location-specific mechanical properties of heart valves.<sup>[17]</sup> Thus, we next explored the capability of combining different patterns into a single tubular structure inspired by the heterogeneous microstructure of the leaflets and interleaflet triangles. This strategy could also potentially be mechano-biologically beneficial to induce and guide the ECM deposition by providing a physiological environment for cells.<sup>[18]</sup> To this end, we developed a customized G-code generator to enable the design of multiphasic MEW scaffolds for deposition on a tubular mandrel with tailored architectures across pre-defined regions. The geometrical features of the valve can be defined by the user across various printing areas (Figure 2a,b). Specifications include the overall valve length, diameter, dimensions of the leaflets as well as the previously used fiber patterns. Various parameters for each of the fiber patterns (see Figure 2h–j) can be further defined, e.g., pore size and number of layers. We and others have previously shown that these parameters enable the fine-tuning of the final mechanical properties of the constructs.<sup>[10e,13,19]</sup> To allow to introduce reinforcement across the interfacial region between the leaflets and the wall, a third region referred to as the Suturing Section can be determined by the user with desired features such as width and pattern design.

In order to validate the new platform, tubular heart valve scaffolds, designed with the dimensions specified in Figure 2b, were successfully fabricated by MEW using a 22 mm diameter mandrel (Figure 2c,d). SEM images of these scaffolds illustrate a highly defined, region-specific architecture with accurately stacked and aligned fibers (Figure 2). Serpentine-like architectures were fabricated for the leaflets of the valve with 1 mm arc diameter, and inter-fiber spacing of 500  $\mu\text{m}$  circumferentially and 2 mm radially following a bioinspired design to mimic the J-shaped stress–strain response of native tissue, as we previously showed for flat scaffolds (Figure 2e,h).<sup>[13]</sup> The choice of fiber architecture for the inter-leaflet triangle is equally complex, as it needs to possess both the strength to support the leaflets,<sup>[20]</sup> as well as adequate flexural properties in the direction of valve open and closure, and compliance in the circumferential direction, similar to the rest of the aorta.<sup>[21]</sup> Thus, a diamond-shaped fiber design was chosen for this region to best recapitulate this behavior, as it possesses higher strength than the serpentine, while still maintaining compliance in both directions (Figure 2f,i). In addition, a rectangular fiber pattern was also designed and fabricated for the inter-leaflet triangle region to demonstrate our ability to alter the different patterns (Figure 2j). Overall, the integration of the novel software and geared mandrel setup allowed for the fabrication of spatially heterogeneous, multiphasic tubular heart valve scaffolds with highly tunable fiber architecture according to the user's input.

### 2.3. Composite MEW/ELR Heart Valve Fabrication and In-Vitro Assessment

Next, we completed the fabrication of the heart valve construct by embedding the macro-porous MEW tubular scaffold into a recombinant elastin-like matrix with controlled micro-porosity. Elastin is an important component of the native ECM of heart valves, which enables their elastic deformation and rapid recoil

during each opening and closing cycle, and thus significantly contributes to the long-term valve functionality.<sup>[22]</sup> ELRs are a class of materials bioinspired by the pentapeptide VPGVG present in human elastin, produced by recombinant technology.<sup>[23]</sup> Chemical modification of the recombinanters with cyclooctyne and azide groups enables the catalyst-free-click chemistry. We had previously taken advantage of this feature to develop a salt leaching/gas foaming method to obtain ELR scaffolds with controlled porosity optimized for cellular infiltration.<sup>[24]</sup> ELRs are excellent biomaterials for cardiovascular applications, because of their low thrombogenicity and their capability to support endothelial layer formation.<sup>[25]</sup> Recent work successfully employed ELRs in an animal model of myocardial infarction, showing complete functional recovery of ejection fraction 21 days after intramyocardial injection, thereby confirming their promising potential for application in the cardiovascular environment.<sup>[26]</sup>

The macro-porous MEW tubular scaffold was composited with ELR via injection molding followed by salt leaching/gas foaming, as schematically illustrated in Figure 3a. The scaffold was positioned in a custom-made mold (Figure 3bi) and the components of the click-ELR were injected. Upon demolding, visual inspection of the composite MEW/ELR heart valve revealed that the MEW scaffold was fully embedded within the ELR (Figure 3bii). This was confirmed by SEM (Figures 3biii). High magnification SEM revealed the highly micro-porous structure of the ELR (Figure 3biv), which is essential to enable fast and adequate cellular infiltration.

In order to assess the acute hemodynamic performance of the composite MEW/ELR heart valves in vitro, constructs were first sutured into custom-made silicone roots. The roots included the sinuses of Valsalva (Figure 3c), thus enabling the simulation of surgical implantation according to the single-point attachment commissure (SPAC) technique.<sup>[27]</sup> The different scaffold regions made the commissures easily identifiable (asterisks in Figure 2f) and thus facilitated the sewing of the construct at these three single attachment points.

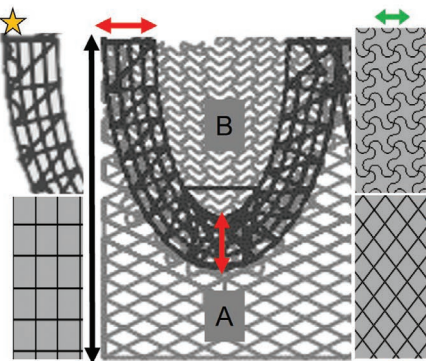
The composite MEW/ELR heart valves were tested according to the ISO 5840 in a custom-made flow loop system, showing unobstructed opening and complete closure during cardiac cycle under aortic and pulmonary conditions (Figures 3d; Video S1 and Figure S2, Supporting Information).

The MEW/ELR heart valve exhibited excellent systolic hemodynamic performance under aortic conditions (Figure 3e) satisfying the ISO standard for a 23 mm valve, with an Effective Orifice Area (EOA) of  $2.12 \text{ cm}^2 \pm 0.12$  (valve diameter: 22 mm) and a mean transvalvular pressure gradient of  $5.00 \pm 0.35 \text{ mm Hg}$ .<sup>[28]</sup> A comparable performance was obtained for the MEW/ELR heart valve tested under pulmonary conditions as indicated by the ISO standard, with an EOA of  $1.97 \text{ cm}^2 \pm 0.05$  and a mean transvalvular pressure gradient of  $6.02 \pm 0.18 \text{ mm Hg}$  (Figure S2, Supporting Information). However, for both aortic and pulmonary conditions, the regurgitant fraction was rather high (14.71% and 14.65%, respectively) and is likely an overestimation of the in vivo regurgitation, due to the porosity of the ELR matrix allowing flow through the leaflets in vitro. We expect this to be a transient issue in vivo, as the scaffold will be immediately infiltrated by blood, and thus sealed upon implantation and, later on, tissue formation will occur. A further reduction of the regurgitant fraction could be achieved by decreasing the closing volume via leaflet

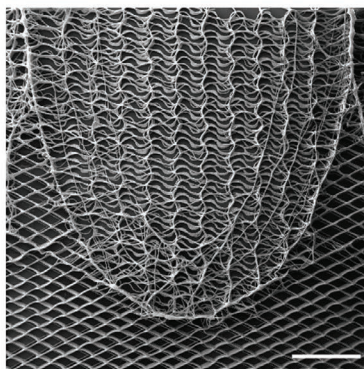
**a**

<b>General Dimensions</b>		<b>Section B Dimensions</b>		<b>Other Dimensions</b>	
Overall Valve Length (mm):	<input type="text" value="32"/>	Section B Pattern:	<input type="text" value="Curves"/>	A Pore Offset (mm):	<input type="text" value="0"/>
Mandrel Diameter (mm):	<input type="text" value="22.5"/>	X Pore Size (mm):	<input type="text" value="1"/>	B Pore Offset (mm):	<input type="text" value="0.02"/>
Number of Layers:	<input type="text" value="5"/>	Y Pore Size (mm):	<input type="text" value="2"/>	Clearance (mm):	<input type="text" value="10"/>
Printing Speed (mm/min):	<input type="text" value="100"/>	X Shape Dimension:	<input type="text" value="1"/>	<b>Coordinates Selection</b>	
Number of Stabilizing Rows:	<input type="text" value="5"/>	Y Shape Dimension:	<input type="text" value="1"/>	Coordinates Type:	<input type="text" value="Global"/>
<b>Suturing Section</b>		Leaflet Length (mm):	<input type="text" value="22"/>	<b>SAVE AS:</b>	<input type="text" value="Valvecode"/>
Suture Thickness (mm):	<input type="text" value="0"/>	<b>Section A Dimensions</b>		<input type="button" value="Generate"/>	
Stitch Length (mm):	<input type="text" value="5"/>	Section A Pattern:	<input type="text" value="Diamonds"/>		
Number of Cross-stitches:	<input type="text" value="20"/>	X Pore Size (mm):	<input type="text" value="2"/>		
Number of Supporting Ribs:	<input type="text" value="5"/>	Y Pore Size (mm):	<input type="text" value="4"/>		
Number of Stitch Layers:	<input type="text" value="3"/>	Extension:	<input type="text" value="1"/>		

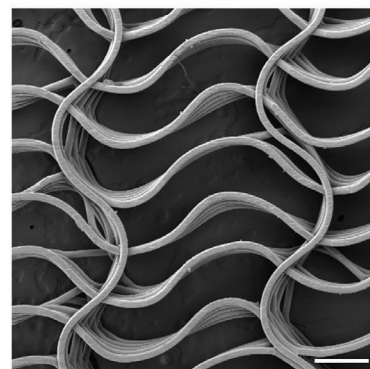
**b**



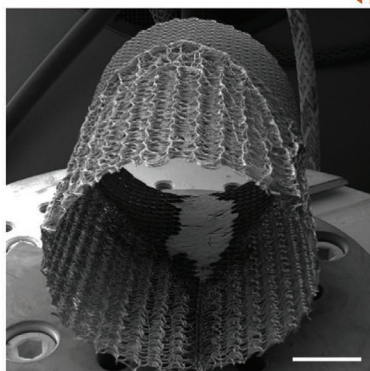
**e**



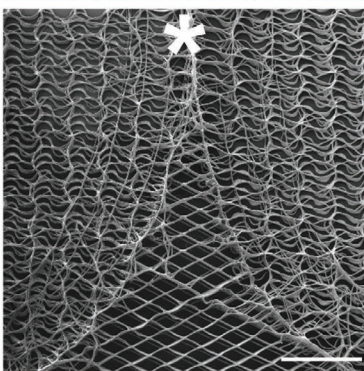
**h**



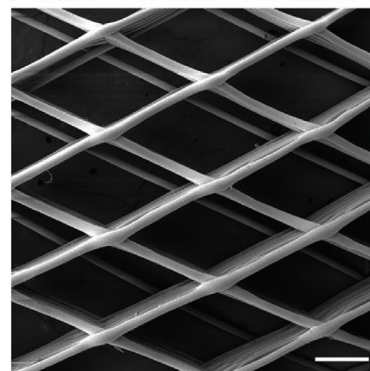
**c**



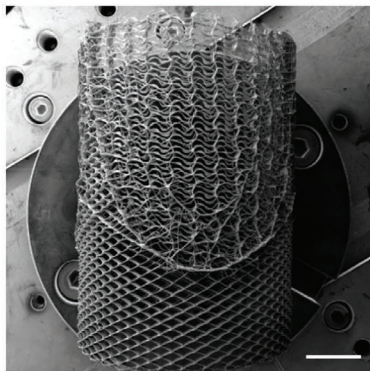
**f**



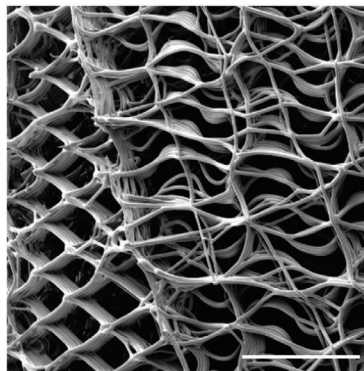
**i**



**d**



**g**



**j**

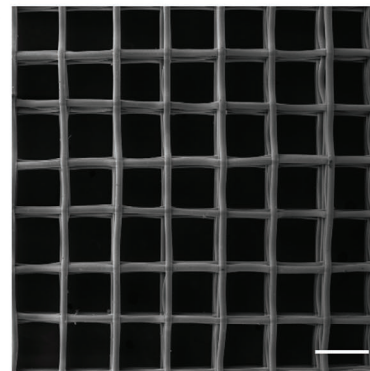


**Figure 2.** Design and fabrication of tubular, spatially heterogeneous, PCL MEW scaffolds for heart valve tissue engineering. a) Graphical user interface of the custom-made G-code generating software. b) Exemplary G-code path of a multiphasic tubular heart valve, generated using the custom G-code generator. c,d) Overview SEM images of spatially heterogeneous scaffolds; scale bar = 5 mm. e–g) Detailed SEM images of interface regions between serpentine and diamond patterns; scale bar e,f = 5 mm, g = 2 mm. h–j) High magnification SEM images of tubular spatially heterogeneous scaffold's individual fiber architectures with serpentine, diamond and rectangular patterns; scale bar = 500  $\mu$ m.

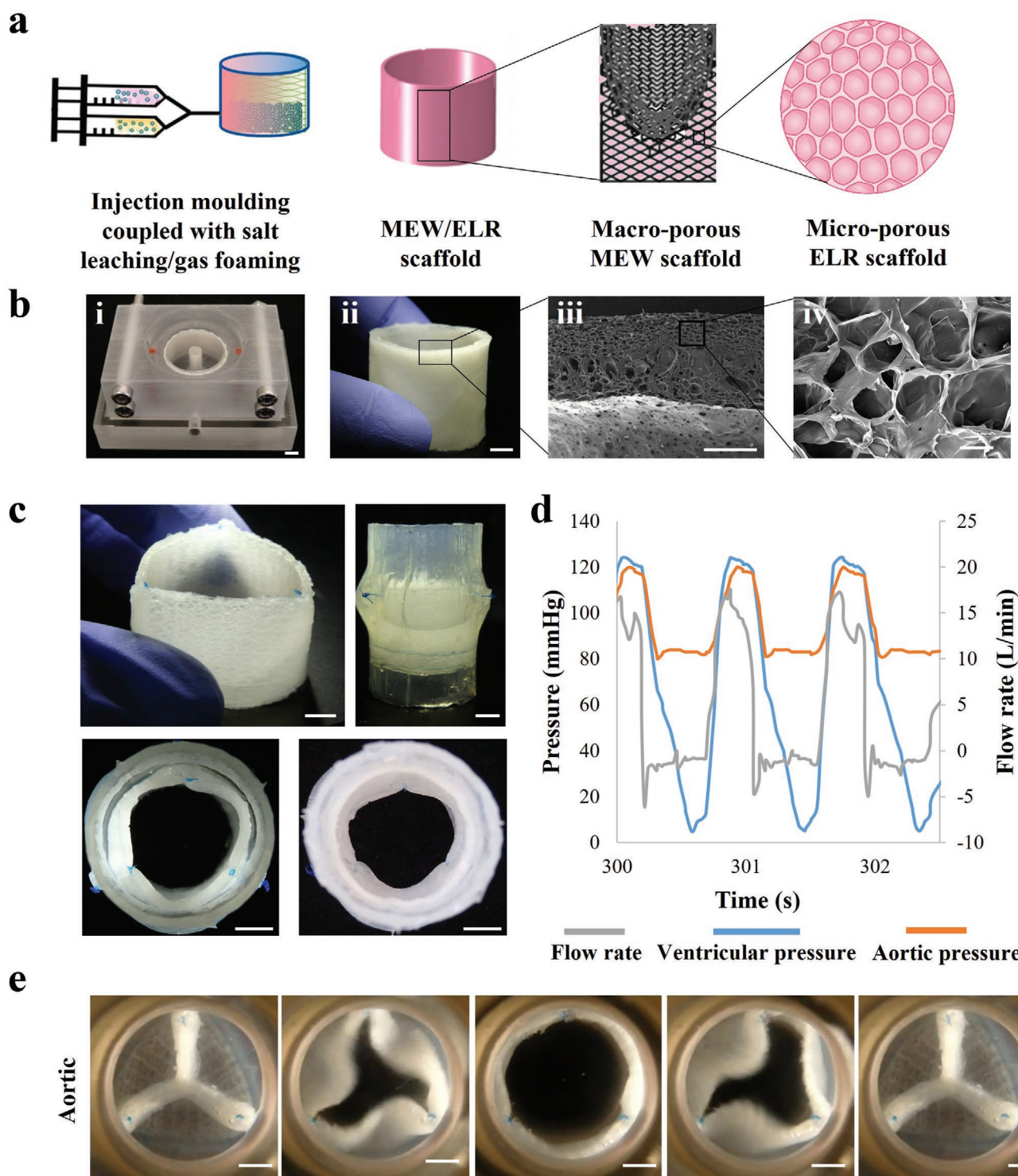


**Figure 3.** a) Schematic of composite MEW/ELR heart valve fabrication and detailed view of their components. b) MEW scaffold embedded via injection molding with ELR and porogen, ii) optical image of composite MEW/ELR heart valve, followed by iii,iv) SEM images at increasing magnification, iii) scale bar 500  $\mu\text{m}$ , iv) scale bar 50  $\mu\text{m}$ . c) Composite MEW/ELR heart valve assembly. d) Pressure and flow measurements during cyclic testing. e) Images of opening and closing cycles using a high-speed camera during flow loop mock circulation system functionality testing under aortic conditions. (Scale bar for all other images: 5 mm).

design optimization. Overall, these results highlight the potential of the composite MEW/ELR heart valve to withstand the physiological hemodynamic conditions necessary for function in both the aortic and pulmonary positions.

While encouraging, they only represent the acute behavior of the valve and are not predictive of its long-term functionality. Ultimately, to validate the proposed concept, after in vitro optimization of the scaffold's design, an in vivo study will be conducted to

evaluate the remodeling process and specifically, the capability of the heterogeneous scaffold architecture and thus resulting in mechanobiological behavior to steer ECM formation. To this end, also the degradation rate of the scaffold will have to be tuned to guide endogenous regeneration towards a native-like matrix composition while, at the same time, continuously providing adequate mechanical stability.<sup>[3a,29]</sup> The degradation behavior of the ELRs can be tailored by inserting protease-sensitive sequences in the protein chain. Specifically, we have shown that by integrating epitopes with different cleavage kinematics and sensitivity to proteolytic cleavage, the degradation rates can be tuned ad hoc.<sup>[30]</sup>

Importantly, the developed fabrication strategy is not limited to the use of ELRs without protease-sensitive sequences as selected for this study, and can benefit from the ever-expanding library of ELRs with tailored functionalities. Furthermore, it can also be translated to other materials and applications. For example, hydrogels such as fibrin<sup>[13]</sup> and star-shaped poly(ethylene glycol)<sup>[31]</sup> have been used, among others, in combination with MEW. PCL is the gold standard for MEW and, although the library of materials is still somehow limited, the increasing interest in this technique has already widened the range of processable polymers,<sup>[32]</sup> including the addition of fillers to increase biofunctionality or mechanical properties for specific applications. We have recently reported PCL MEW-scaffolds made visible in MRI by incorporation of ultra-small paramagnetic iron oxide particles (USPIOs) with the idea of facilitating their clinical translation.<sup>[10c]</sup> We have also developed a method to process poly(L-lactide-co-ε-caprolactone) (PLCL) via MEW.<sup>[33]</sup> PLCL is an elastic polymer with relatively fast degradation profile and is commercially available in high purity, properties that make it interesting for, e.g., heart valve tissue engineering.

### 3. Conclusion

We present a newly developed MEW platform that enables the digital fabrication of tubular scaffolds with spatially heterogeneous, highly tunable, and precise fiber architectures for HVTE. The region-specific MEW tubular scaffolds were composited with a microporous ELR matrix, together providing both the structural integrity required to withstand the demanding cardiovascular loading conditions and adequate porosity to enable cell infiltration. Composite MEW/ELR heart valves present significant advantages for an off-the-shelf solution for in situ HVTE, a promising avenue forward in the field of HVTE due to the reduced regulatory and logistical hurdles toward clinical translation,<sup>[28b]</sup> as the suboptimal structural properties of dense fibrous scaffolds to date are a major issue jeopardizing their clinical potential. In summary, our platform facilitates a new paradigm for the digital manufacture of composite MEW/ELR heart valves for in situ HVTE that could also be extended to other soft tissue engineering applications.

### 4. Experimental Section

**G-code Generation:** G-code for single-phasic tubular structures of a specified scaffold diameter and length were designed using a proprietary MATLAB G-code generation software, accommodating transversely-positioned rectangle-, diamond-, and serpentine-architecture fibers. The G-code generation software allowed independently tunable fiber spacing, transverse angle, and, where appropriate, diameter and curvature degree

of serpentine fibers. For multiphasic structures, a second proprietary G-code generator was developed to design the deposition of fibers for the leaflets, inter-leaflet triangles, the region between these two, as well as the annulus. For each region, length, fiber architecture (including rectangle, serpentine, and diamond), and independent layer numbers could be defined. Two G-codes were generated for continuous printing of the entire structure including the leaflets, inter-leaflet triangles, and aortic root.

**Manufacturing of MEW Scaffolds and MEW/ELR Composite Tubes:** Tubular single- and multiphasic scaffolds were fabricated in medical-grade PCL (Purasorb PC 12, Corbion, The Netherlands) using an in-house-built MEW device, with regulated air pressure-driven extrusion at 2 bar through a 23G metallic needle on a motorized mandrel collector integrated with custom gearing system for improved resolution on mandrel collection. A working distance of 3 mm was used with 100 mm min<sup>-1</sup> translation speed and voltage of 3.6 kV applied to the spinneret and grounded collector plate. For the fabrication of the MEW/ELR composite, a structural and a bioactive ELR modified as previously reported<sup>[34]</sup> were used at their lysine aminoacids with cyclooctyne and azide groups required for the catalyst-free-click chemistry reaction. Specific information on the ELRs (i.e., the amino acid sequence, molecular weight, number of amino acids and modification degree with cyclooctyne and azide groups) is listed in **Table 1**. A recently developed injection molding coupled with salt leaching/gas foaming technique was applied.<sup>[24]</sup> Briefly, each ELR component was dissolved at 75 mg mL<sup>-1</sup> in a 1:1 (v/v) mixture of phosphate buffer saline (PBS) and ethanol. NaHCO<sub>3</sub> particles (diameter < 100 μm) were added to each ELR solution at a recombinamer/salt weight ratio of 1:10. Each preparation was loaded into a syringe for subsequent injection into a custom-made mold using a dual chamber syringe applicator.

The mold consisted of a main base, inner cylinder, and two outer shells. The MEW scaffold was placed around the inner cylinder in a pre-designed ridge followed by assembly of the outer shells ensuring the even placement of the scaffold in the composite. Both ELR preparations were injected into the mold with a mixing nozzle and left to polymerize for 30 min at 37 °C. The cross-linked ELR hydrogel embedded with the MEW scaffold was then removed from the mold and placed in 3 M citric acid for 30 min in an ultrasound bath. The scaffolds were washed with aqueous PBS.

**Scanning Electron Microscopy and Morphological Analysis:** Scaffolds were gold sputter-coated (JEOL fine sputter coater) for 150 s at 10 mA and full multiphasic scaffolds were titanium coated prior to imaging. Following printing and removal of scaffolds from the mandrel, macroscopic images of the single-phasic scaffolds were acquired with (Nikon DS-Fi2, Japan). Scanning electron micrographs of entire scaffolds and representative regions of unit cell designs were acquired with a TESCAN Mira3 SEM (Brno, Czechia) using 8.00 beam intensity, 5.0 kV of voltage. Morphological quantification of fiber orientation was performed using OrientationJ plugin (ImageJ, NIH).

**Biaxial Mechanical Characterization:** Biaxial tensile testing was performed on scaffolds using the Biotester (Cellscale, Waterloo, Canada) equipped with a 5 N load cell. Samples ( $n = 4$  for each pattern) were secured with clamps and suspended in air at room temperature. A tensile strain of 100% of the scaffold's length was applied at a displacement rate of 3% length min<sup>-1</sup> and a stress-strain curve was plotted to characterize the scaffold under tensile loading and recovery. Linear elastic modulus was calculated from the slope of the stress-strain curve at the steepest

**Table 1.** Specifications of the used ELRs.

	VKV24	HRGD6
Sequence	MESLLP VG VPGVG [VPGKG (VPGVG)] <sub>3</sub> <sub>23</sub> VPGKG VPGVG VPGVG VPGVG VPGV	MGSSHHHHHHSSGLVPR GSHMESLLP (((VPGIG)2(VPGKG)(VPGIG)) <sub>2</sub> ) <sub>2</sub> AVTGRGDSPASS [(VPGIG) <sub>2</sub> VPGKG (VPGIG) <sub>2</sub> ] <sub>6</sub> V
MW [Da]	60 450.91	60 649.90
N [aas]	727	699
Modification	16 Lys modified with cyclooctyne	16 Lys modified with azide



region, the strain range for which varied between 2% and 23%, depending on the sample/pattern. Ultimate tensile strength was determined as the maximum stress reached for each sample. Displayed bar charts are mean values. Error bars represent standard deviation. Multiple, unpaired, parametric, Welch *t*-tests were performed using GraphPad Prism software (GraphPad, San Diego, USA). Additional statistical analyses comparing both linear elastic modulus and ultimate tensile strength between various fiber architectures are displayed in Figure S3 (Supporting Information).

**Heart Valve Assembly and In Vitro Functional Characterization in Mock Circulation System:** Assembly of the complete heart valves was achieved by pinching the three commissural points of the scaffolds using sutures (Prolene 4-0; Ethicon GmbH). These points were then fixed inside custom-made silicon roots between the sinuses of Valsalva using sutures, as well as an additional suture around the circumference of the annulus. An in-house flow loop circulation device was used to characterize the functionality of the scaffolds under both pulmonary and aortic conditions. MEW/ELR tubular heart valves were mounted into a custom-built holder that allowed for the circulation of distilled water at a flow rate of 5 L min<sup>-1</sup>, driven by a pneumatic pressurized film at a 70 bpm frequency. Heart valves were tested at aortic condition (mean aortic pressure 100 mm Hg, 120–80 mm Hg), in accordance with ISO 5840–2 guidelines. A flowmeter (sonoTT, em-tec GmbH) was used to measure the instantaneous inflow to the valve and pressure transducers (DPT 6000, pvd CODAN Critical Care GmbH) were placed at the inflow and outflow side of the valve to measure the pressure.

## Supporting Information

Supporting Information is available from the Wiley Online Library or from the author.

## Acknowledgements

E.M.D.P. and P.M. contributed equally to this work. The authors gratefully acknowledge the financial support of the Australian Research Council (ARC ITTC in Additive Biomanufacturing, IC160100026), the Centre in Regenerative Medicine (IHBI, QUT), the German Research Foundation (DFG – Project number: 403170227 ArchiTissue), the START-Program of the Medical Faculty of RWTH Aachen University (60/17)), the Spanish Government (PID2019-110709RB-I00, RED2018-102417-T), Junta de Castilla y León (VA317P18, Infrared2018-UVA06), Interreg V España Portugal POCTEP (0624\_2IQBIONEURO\_6\_E) and Centro en Red de Medicina Regenerativa y Terapia Celular de Castilla y León. SEM imaging of MEW scaffolds was performed at the Central Analytical Research Facility operated by the Institute for Future Environments and supported by Science and Engineering Faculty at QUT.

Open access funding enabled and organized by Projekt DEAL.

## Conflict of Interest

The authors declare no conflict of interest.

## Data Availability Statement

The data that support the findings of this study are available from the corresponding author upon reasonable request.

## Keywords

elastin-like, heart valves, heterogeneous tubular scaffolds, in situ tissue engineering, melt electrowriting

Received: October 22, 2021

Revised: December 31, 2021

Published online: February 15, 2022

- [1] a) A. Sanz-Garcia, J. Oliver-de-la-Cruz, V. Mirabet, C. Gandia, A. Villagrasa, E. Sodupe, C. Escobedo-Lucea, *Expert Rev Mol Med* **2015**, *17*, e16; b) S. S. Virani, A. Alonso, H. J. Aparicio, E. J. Benjamin, M. S. Bittencourt, C. W. Callaway, A. P. Carson, A. M. Chamberlain, S. Cheng, F. N. Delling, M. S. V. Elkind, K. R. Evenson, J. F. Ferguson, D. K. Gupta, S. S. Khan, B. M. Kissela, K. L. Knutson, C. D. Lee, T. T. Lewis, J. Liu, M. S. Loop, P. L. Lutsey, J. Ma, J. Mackey, S. S. Martin, D. B. Matchar, M. E. Mussolino, S. D. Navaneethan, A. M. Perak, G. A. Roth, et al., *Circulation* **2021**, *143*, e254.
- [2] I. Vesely, *Circ. Res.* **2005**, *97*, 743.
- [3] a) T. B. Wissing, V. Bonito, C. V. C. Bouten, A. Smits, *NPJ Regen Med* **2017**, *2*, 18; b) F. Zafar, D. L. S. Morales, *J. Thorac. Cardiovasc. Surg.* **2018**, *155*, 2602.
- [4] a) J. T. Butcher, *Sci. Transl. Med.* **2018**, *10*, eaat5850; b) R. L. Li, J. Russ, C. Paschalides, G. Ferrari, H. Waisman, J. W. Kysar, D. Kalfa, *Biomaterials* **2019**, *225*, 119493.
- [5] a) J. Kluin, H. Talacua, A. I. Smits, M. Y. Emmert, M. C. Brugmans, E. S. Fioretta, P. E. Dijkman, S. H. Sontjens, R. Duijvelshoff, S. Dekker, M. W. Janssen-van den Broek, V. Lintas, A. Vink, S. P. Hoerstrup, H. M. Janssen, P. Y. Dankers, F. P. Baaijens, C. V. Bouten, *Biomaterials* **2017**, *125*, 101; b) V. Ballotta, A. Driessen-Mol, C. V. Bouten, F. P. Baaijens, *Biomaterials* **2014**, *35*, 4919.
- [6] M. Uiterwijk, A. Smits, D. van Geemen, B. van Klarenbosch, S. Dekker, M. J. Cramer, J. W. van Rijswijk, E. B. Lurier, A. Di Luca, M. C. P. Brugmans, T. Mes, A. W. Bosman, E. Aikawa, P. F. Grundeman, C. V. C. Bouten, J. Kluin, *JACC Basic Transl Sci* **2020**, *5*, 1187.
- [7] P. Mela, A. D'Amore, *JACC Basic Transl Sci* **2020**, *5*, 1207.
- [8] A. D'Amore, S. K. Luketich, G. M. Raffa, S. Olia, G. Menallo, A. Mazzola, F. D'Accardi, T. Grunberg, X. Gu, M. Pilato, M. V. Kameneva, V. Badhwar, W. R. Wagner, *Biomaterials* **2018**, *150*, 25.
- [9] S. Jana, A. Lerman, *Cell Tissue Res.* **2020**, *382*, 321.
- [10] a) M. von Witzleben, T. Stoppe, T. Ahlfeld, A. Bernhardt, M. L. Polk, M. Bornitz, M. Neudert, M. Gelinsky, *Adv. Healthcare Mater.* **2021**, *10*, 2002089; b) N. T. Saidy, T. Shabab, O. Bas, D. M. Rojas-Gonzalez, M. Menne, T. Henry, D. W. Hutmacher, P. Mela, E. M. De-Juan-Pardo, *Front Bioeng Biotechnol* **2020**, *8*, 793; c) K. M. A. Mueller, G. J. Topping, S. P. Schwaminger, Y. Zou, D. M. Rojas-Gonzalez, E. M. De-Juan-Pardo, S. Berensmeier, F. Schilling, P. Mela, *Biomater. Sci.* **2021**, *9*, 4607; d) A. Hrynevich, P. Achenbach, T. Jungst, G. A. Brook, P. D. Dalton, *Macromol. Biosci.* **2021**, *21*, 2000439; e) A. Shafiee, A. S. Cavalcanti, N. T. Saidy, D. Schneider, O. Friedrich, A. Ravichandran, E. M. De-Juan-Pardo, D. W. Hutmacher, *Biomaterials* **2021**, *268*, 120558.
- [11] a) L. C. Martine, B. M. Holzapfel, J. A. McGovern, F. Wagner, V. M. Quent, P. Hesami, F. M. Wunner, C. Vaquette, E. M. De-Juan-Pardo, T. D. Brown, B. Nowlan, D. J. Wu, C. O. Hutmacher, D. Moi, T. Oussenko, E. Piccinini, P. W. Zandstra, R. Mazziere, J. P. Levesque, P. D. Dalton, A. V. Taubenberger, D. W. Hutmacher, *Nat. Protoc.* **2017**, *12*, 639; b) B. A. Pereira, N. L. Lister, K. Hashimoto, L. Teng, M. Flandes-Iparraguirre, A. Eder, A. Sanchez-Herrero, B. Niranjana, A. Melbourne Urological Research, *Biomaterials* **2019**, *197*, 72.
- [12] a) T. Jungst, M. L. Muerza-Cascante, T. D. Brown, M. Standfest, D. W. Hutmacher, J. Groll, P. D. Dalton, *Polym. Int.* **2015**, *64*, 1086; b) T. D. Brown, A. Slotosch, L. Thibaudeau, A. Taubenberger, D. Loessner, C. Vaquette, P. D. Dalton, D. W. Hutmacher, *Biointerphases* **2012**, *7*, 13.
- [13] N. T. Saidy, F. Wolf, O. Bas, H. Keijden, D. W. Hutmacher, P. Mela, E. M. De-Juan-Pardo, *Small* **2019**, *15*, 1900873.
- [14] E. O. Carew, A. Garg, J. E. Barber, I. Vesely, *Ann. Biomed. Eng.* **2004**, *32*, 563.
- [15] M. S. Sacks, W. David Merryman, D. E. Schmidt, *J. Biomech.* **2009**, *42*, 1804.
- [16] a) M. S. Sacks, A. P. Yoganathan, *Philos Trans R Soc Lond B Biol Sci* **2007**, *362*, 1369; b) N. Latif, P. Sarathchandra, P. M. Taylor, J. Antoni, M. H. Yacoub, *J. Heart Valve Dis.* **2005**, *14*, 218.

- [17] a) A. Balguid, N. J. Driessen, A. Mol, J. P. Schmitz, F. Verheyen, C. V. Bouten, F. P. Baaijens, *J. Biomech.* **2008**, *41*, 2612; b) G. Marom, M. Peleg, R. Halevi, M. Rosenfeld, E. Raanani, A. Hamdan, R. Haj-Ali, *J. Biomech. Eng.* **2013**, *135*, 101001.
- [18] M. A. Cox, J. Kortsmit, N. Driessen, C. V. Bouten, F. P. Baaijens, *Tissue Eng Part A* **2010**, *16*, 1527.
- [19] G. Hochleitner, F. Chen, C. Blum, P. D. Dalton, B. Amsden, J. Groll, *Acta Biomater.* **2018**, *72*, 110.
- [20] J. P. Sutton, III, S. Y. Ho, R. H. Anderson, *Ann. Thorac. Surg.* **1995**, *95*, 419.
- [21] a) D. A. Vorp, B. J. Schiro, M. P. Ehrlich, T. S. Juvonen, M. A. Ergin, B. P. Griffith, *Ann. Thorac. Surg.* **2003**, *75*, 1210; b) E. M. Joyce, J. Liao, F. J. Schoen, J. E. Mayer, Jr., M. S. Sacks, *Ann. Thorac. Surg.* **2009**, *87*, 1240.
- [22] K. M. Kodigepalli, K. Thatcher, T. West, D. P. Howsmon, F. J. Schoen, M. S. Sacks, C. K. Breuer, J. Lincoln, *J. Cardiovasc. Dev. Dis.* **2020**, *7*, 57.
- [23] A. Girotti, A. Fernandez-Colino, I. M. Lopez, J. C. Rodriguez-Cabello, F. J. Arias, *Biotechnol. J.* **2011**, *6*, 1174.
- [24] A. Fernandez-Colino, F. Wolf, H. Keijdener, S. Rutten, T. Schmitz-Rode, S. Jockenhoewel, J. C. Rodriguez-Cabello, P. Mela, *Mater Sci Eng C Mater Biol Appl* **2018**, *88*, 140.
- [25] a) I. G. de Torre, F. Wolf, M. Santos, L. Rongen, M. Alonso, S. Jockenhoewel, J. C. Rodriguez-Cabello, P. Mela, *Acta Biomater.* **2015**, *12*, 146; b) A. Fernandez-Colino, F. Wolf, S. Rutten, T. Schmitz-Rode, J. C. Rodriguez-Cabello, S. Jockenhoewel, P. Mela, *Front Bioeng Biotechnol* **2019**, *7*, 340.
- [26] P. Contessotto, D. Orbanic, M. Da Costa, C. Jin, P. Owens, S. Chantepie, C. Chinello, J. Newell, F. Magni, D. Papy-Garcia, N. G. Karlsson, M. Kilcoyne, P. Dockery, J. C. Rodriguez-Cabello, A. Pandit, *Sci. Transl. Med.* **2021**, *13*, eaaz5380.
- [27] W. A. Goetz, T. E. Tan, K. H. Lim, H. Salgues Sle, N. Grousson, F. Xiong, Y. L. Chua, J. H. Yeo, *Eur. J. Cardiothorac. Surg.* **2008**, *33*, 548.
- [28] a) C. Dal Lin, T. Bottio, E. Buratto, V. Tarzia, G. Rizzoli, V. Savona, G. Gerosa, *J. Heart Valve Dis.* **2012**, *21*, 112; b) C. V. C. Bouten, A. Smits, F. P. T. Baaijens, *Front. Cardiovasc. Med.* **2018**, *5*, 54.
- [29] W. Wu, R. A. Allen, Y. Wang, *Nat. Med.* **2012**, *18*, 1148.
- [30] a) T. Flora, I. Gonzalez de Torre, M. Alonso, J. C. Rodriguez-Cabello, *Biofabrication* **2019**, *11*, 035008; b) F. Gonzalez-Perez, A. Ibanez-Fonseca, M. Alonso, J. C. Rodriguez-Cabello, *Acta Biomater.* **2021**, *130*, 149.
- [31] O. Bas, E. M. De-Juan-Pardo, C. Meinert, D. D'Angella, J. G. Baldwin, L. J. Bray, R. M. Wellard, S. Kollmannsberger, E. Rank, C. Werner, T. J. Klein, I. Catelas, D. W. Hutmacher, *Biofabrication* **2017**, *9*, 025014.
- [32] J. C. Kade, P. D. Dalton, *Adv. Healthcare Mater.* **2021**, *10*, 2001232.
- [33] R. Sanchez Diaz, J.-R. Park, L. L. Rodrigues, P. D. Dalton, E. M. De-Juan-Pardo, T. R. Dargaville, *Adv. Mater. Technol.* **2021**.
- [34] I. Gonzalez de Torre, M. Santos, L. Quintanilla, A. Testera, M. Alonso, J. C. Rodriguez Cabello, *Acta Biomater.* **2014**, *10*, 2495.